The Mode of Action of Phospholipase A_2: Semiempirical MO Calculations Including the Protein Environment

Gudrun Schürer, Harald Lanig, and Timothy Clark*

Computer-Chemie-Centrum der Friedrich-Alexander-Universität Erlangen-Nürnberg, Nägelsbachstrasse 25, D-91052 Erlangen, Germany

Received: September 17, 1999; In Final Form: November 30, 1999

Phospholipase A_2 is a calcium-dependent enzyme involved in inflammatory processes by releasing arachidonic acid from the sn-2 position of phosphatidyl-cholines. The catalyzed reaction is an ester hydrolysis that takes place in two proton transfer steps via an intermediate. Two mechanisms, which differ mainly in the rate-limiting step, have been proposed in the literature. The reaction has been calculated semiempirically (PM3) for a protein fragment containing the active site (156 atoms). To take long-range electrostatic interactions of the protein bulk with the active site into account, a classical-mechanical protein environment has been provided by a rigid point-charge array with associated van der Waals potentials. In this way a model system has been built that simulates the natural situation in an enzyme more realistically than a pure model of the active site. A comparison between the relative energy paths obtained by calculating the reaction in the isolated active site and within the classical mechanical environment shows that the long-range interactions have a strong influence on the mechanism. While the calculations of the smaller system indicate that the first reaction step, the formation of the intermediate, is rate-limiting, the calculations including the protein environment show that the decomposition of the intermediate is probably rate-limiting. The results clearly show that the protein environment cannot be disregarded during quantum-mechanical calculations of enzyme mechanisms.

Introduction

The theoretical treatment of biological systems such as enzymes is of considerable interest. Microscopic details of modes of action that are not accessible by any other methods can be determined, and clear choices between two or more reaction paths that are indistinguishable by experiment are possible. However, the size of proteins makes pure quantum-mechanical calculations difficult. The active site of enzymes can be treated separately with semiempirical methods, but this implies that the long-range interactions with the protein environment are ignored. However, electrostatic effects are thought to be the most important factor in enzyme catalysis, along with hydrophobic or entropic effects.[1] Thus, intermediates whose lifetimes in solution would be too short to allow a further reaction, or transition states can be stabilized by electrostatic interactions with the protein environment. To be able to address this type of problem, a number of mixed quantum-mechanics/molecular-mechanics (QM/MM) approaches have been developed.[2−6] Using these techniques for studies on enzymes, the protein environment is treated classically and the reaction center quantum-mechanically. In this way protein-environment effects can be included with acceptable computational costs. QM/MM methods have been used successfully for the investigation of enzyme reaction mechanisms by several reasearch groups,[7−16] and reviews on this topic are available in the literature.[17−19]

Phospholipase A_2, the subject of this work, has also been studied previously with QM/MM methods. Waskowycz et al. used ab initio QM/MM calculations to investigate the potential energy surface of the ester hydrolysis.[20] A mixed QM/MM method has also been used for molecular dynamics (MD) simulations. Bala et al. combined a quantum-classical molecular dynamics model (QCMD) with a valence bond (VB) method[21] to simulate the enzymatic reaction of PLA_2.[22,23] They adopted the basic scheme of the empirical valence bond (EVB) method,[24] but used data obtained from quantum-mechanical calculations for the parameterization.

We earlier investigated the cleavage of the sn-2 ester bond by PLA_2 with different model systems[25] on a pure semiempirical basis. We showed that a simplified model of the active site together with weak harmonic constraints to conserve the basic geometry provides much more realistic results than a minimal model containing only the reaction partners. We now place the quantum-mechanically treated active site model inside a classical protein environment[26] in order to simulate the Coulombic and van der Waals interactions between the active site and the bulk of the enzyme. A comparison of the relative energies of the activation barriers and the reaction intermediates of different model systems with increasing size allows us to investigate the effects of the protein environment on the enzyme reaction and gives further insight into the catalytic mechanism of the protein.

The System Investigated

For phospholipase A_2 (E.C.3.1.1.4) three isoforms are known. Two of them, secretory ($sPLA_2$) and cytosolic ($cPLA_2$) are calcium-dependent. The function of the calcium-independent third isoform ($iPLA_2$) is still unknown, while $sPLA_2$ and $cPLA_2$ are both involved in inflammatory processes by releasing arachidonic acid from the sn-2 position of phosphatidyl-cholines. They are therefore targets for new anti-inflammatory drugs. Between 40 and 50 inhibitors have been described for $sPLA_2$ over the past decade.[27]

* Corresponding author e-mail: clark@chemie.uni-erlangen.de

10.1021/jp993330i CCC: $19.00
Published on Web 01/21/2000

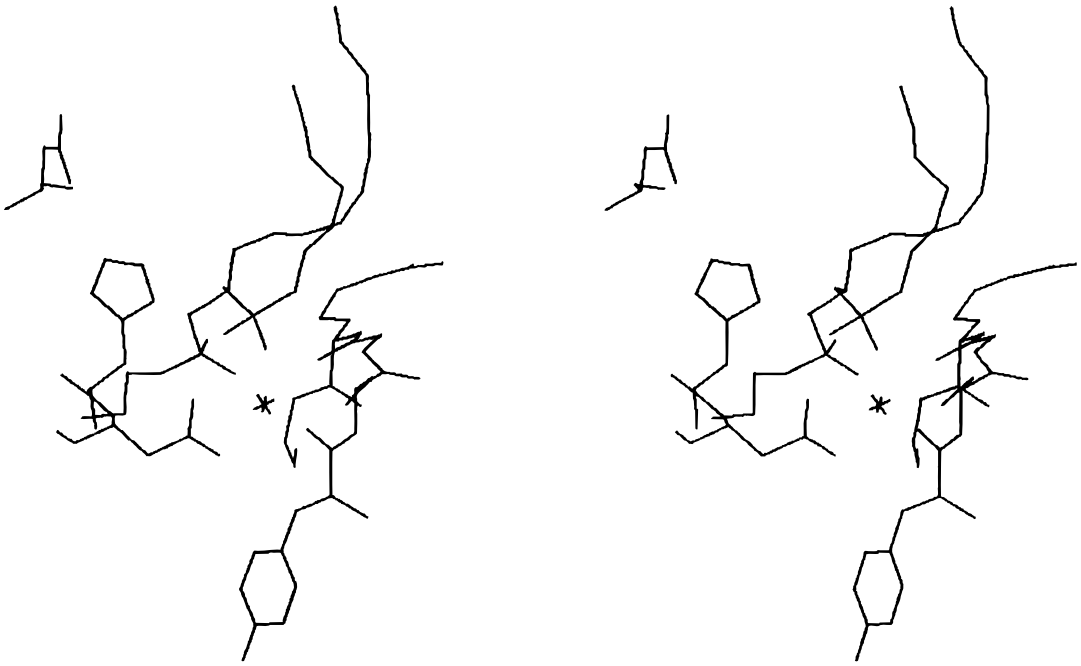

Figure 1. Stereoplot of the active site of PLA_2 complexed with a transition state analogue (PDB entry: 1pob). On the right side of the Ca^{2+} ion the calcium-binding loop is shown (Tyr28, Cys29, Gly30, Arg31, and Gly32) which is coordinated to the metal ion by the carbonyl oxygen atoms of Tyr28, Gly30, and Gly32. On the left side are the residues His48 and Asp49 (coordinated by both carboxylate oxygen atoms of Asp49). His48 is hydrogen bonded to Asp99. The inhibitor lies above the Ca^{2+} ion and is coordinated by the carbonyl oxygen of the sn2 ester group and an oxygen of the phosphate group.

A peculiarity of PLA_2 is the interfacial activation. This means that its activity toward aggregated substrates is considerably higher than that toward monomeric substrate molecules.[28] Recently this phenomenon was used in nanotechnology by combining PLA_2 with an atomic force microscope (AFM). This method, known as enzyme-assisted nanoscale lithography, was used for the local hydrolysis of phospholipid membranes. In this way, investigations and manipulations of surfaces on the nanometer-length scale are possible for biological surfaces, such as cell membranes.[29]

The active site residues in all known $sPLA_2$'s are highly conserved.[30] The active site, shown in Figure 1, contains a Ca^{2+} ion coordinated by three carbonyl oxygen atoms in a calcium-binding loop (Tyr28, Gly30, Gly32),[31] Asp49 as a bidentate ligand and two water molecules in the free enzyme or the inhibitor and substrate, respectively. The amide hydrogen atoms of the residues Gly30 and Gly32 form hydrogen bonds to the phosphate group and the charged sn-2 group of the tetrahedral intermediate of the inhibitor/substrate, so that the correct orientation of the ligand is stabilized. The highly conserved His48 is located next to the active site and is hydrogen bonded to the likewise highly conserved Asp99 via nitrogen Nϵ2. In this way, the active site is connected via a hydrogen bond network with the N terminus (Ala1) of the protein, which is an important residue for interfacial catalysis.[32−35] Beside its catalytic function, Asp99 is proposed to play a role in structural conservation.[36,37]

Calcium is essential for the catalytic activity of PLA_2. Its suggested function is to bind the substrate and to polarize its coordinated carbonyl group in order to facilitate the hydrolysis.[38] It is also proposed to provide a suitable conformation of the active and the substrate binding sites,[39] to play a role in stereoselectivity,[40] and to bind the nucleophilic water within its coordination shell,[41] so that the deprotonation of the water molecule is facilitated and a OH^- ion is obtained as the nucleophilic.[42]

Calcium ions prefer large and asymmetrical coordination geometries.[43] Crystal structures of PLA_2 show that the active site calcium is heptacoordinated in a pentagonal bipyramid. In the free enzyme the equatorial positions are occupied with Oδ1 and Oδ2 of Asp49, the carbonyl oxygen atoms of Gly30 and Gly32 and a water molecule. The carbonyl oxygen of Tyr28 and another water molecule are placed in the axial positions.[44] In most calcium-containing enzymes the coordination number is seven, eight, or nine.[43] Therefore, it is possible that the coordination sphere of the active site calcium in PLA_2 can be extended during the hydrolysis reaction from seven to eight or even nine ligands.

The Protein DataBank[45] contains several X-ray structures of the protein from different sources. We have used the PLA_2 of the venom of the Taiwan Cobra, which is a Type II $sPLA_2$. The coordinates are available as PDB entries 1poa (the free enzyme) and 1pob (in complex with a transition state analogue).[46]

The Catalytic Mechanisms

Based on crystal structures, Verheij et al. proposed a catalytic mechanism (Figure 2) that can be called the "catalytic triad" mechanism, because of its similarity to serine proteases.[38,44,47] Asp99, His48, and the nucleophilic water present in the active site build a catalytic triad similar to the well-known one in serine proteases.[32,48] The nucleophilic water attacks the carbonyl carbon of the sn-2 ester group of the substrate and forms the tetrahedral intermediate. During this step, His48 is protonated at Nδ1. The positively charged His48 in the tetrahedral intermediate complex is stabilized by the interaction with the negatively charged Asp99. Finally the decomposition of the tetrahedral intermediate gives an alcoholate, which is in turn protonated by His48. The role of the calcium ion in the "catalytic triad" mechanism is to bind the substrate and to polarize the carbonyl carbon of the sn-2 ester group. It is not involved directly in the catalytic mechanism.

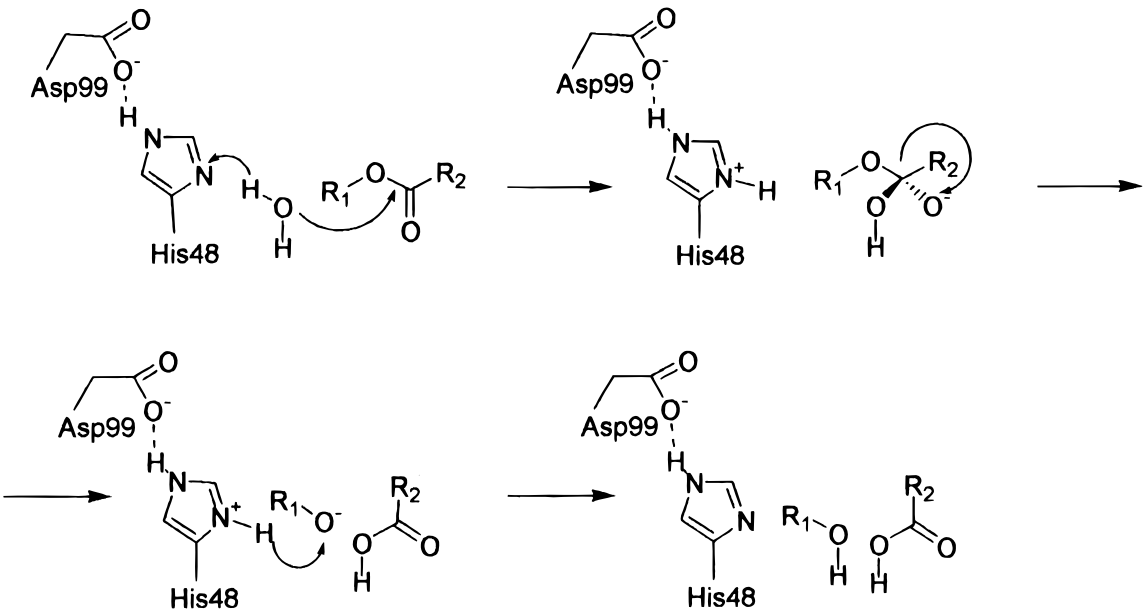

Figure 2. The "catalytic triad" mechanism, as commonly known from the serine proteases. The function of the serine residue is taken over by one water molecule.

However, some experimental results cannot be explained sufficiently by this mechanism. Kinetic studies on mutants, where Asp99 has been substituted by neutral Asn, have shown that the effect of Asp99 on the catalytic activity is less than that of the corresponding Asp in serine proteases. The activity of the D99N mutant of PLA_2 decreases by a factor of about 20 compared to the wild-type PLA_2, whereas the decrease factor of the D102N mutant of the serine protease Trypsin is about 10^4.[49] This indicates that the role of Asp99 is not as important as that of the comparable Asp residues in serine proteases.

Furthermore, the ratio of activity between substrates containing an ester group in the sn2 position and analogous thioesters is about 10.[50] Since a nucleophilic attack on a thioester should be faster than on a normal ester, the formation of the tetrahedral intermediate cannot be rate-limiting.[51]

Recently an alternative mechanism[42,50,52,53] has been suggested, in which the rate-determining step is not the formation of the tetrahedral intermediate, but its decomposition, which is proposed to be influenced by the polar headgroup of the phospholipid coordinated to the calcium ion. This suggestion is based on kinetic studies with different headgroups.[50]

This mechanism differs from the "catalytic triad" mechanism by involving two different water molecules. One (H_2O (1) in Figure 3) is deprotonated and forms the nucleophilic OH^-, while the other (H_2O (2) in Figure 3) is hydrogen bonded to His48 and accepts the proton from the first water molecule. The hydroxide ion is coordinated to the calcium ion, increasing the calcium coordination number to eight. This mechanism, shown in Figure 3, has been called the "calcium-coordinated oxyanion" mechanism,[42] but is closely analogous to the general base mechanism found quite generally for zinc enzymes.[54−58] It is made consistent with the experimental results by claiming the decomposition as the rate-limiting step. In this way residual catalytic activity of the D99N mutant can be explained, because Asp99 facilitates the formation of the tetrahedral intermediate, which is no longer rate-determining.

The coordination behavior of calcium ions also supports the oxyanion mechanism. Calcium easily coordinates up to nine ligands. The substitution of calcium by cadmium, which has a comparable charge and radius but prefers a different coordination geometry, leads to an activity of about one percent

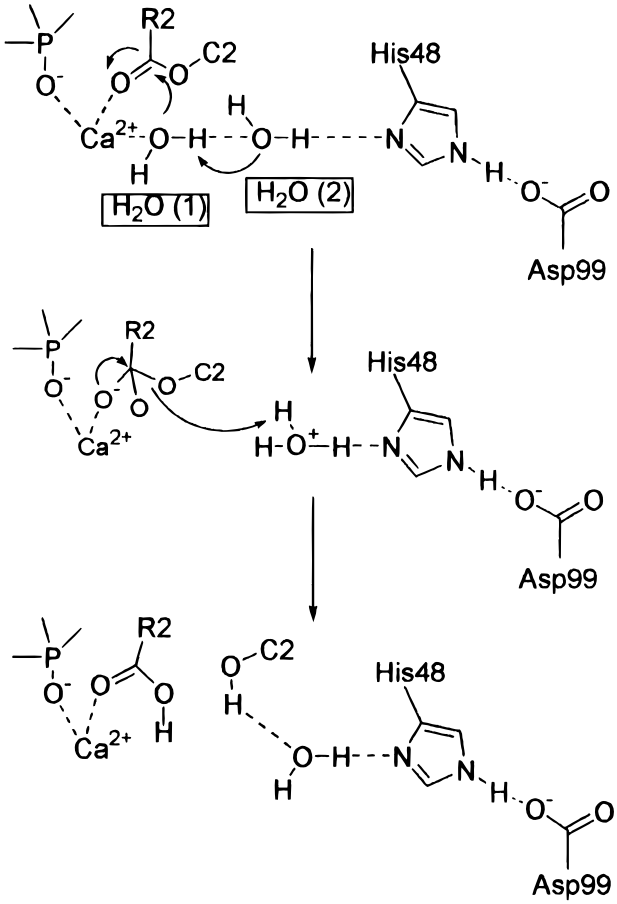

Figure 3. The "calcium-coordinated oxyanion" mechanism, as a second possibility for the cleavage of phospholipids using two water molecules.

compared to the calcium-containing enzyme, although no evidence for conformational changes was observed experimentally.[59] If the only function of the metal ion is to bind the substrate and to polarize the carbonyl group, as proposed by Verheij,[38] cadmium should be a satisfactory substitute. Yu suggested that the coordination geometry of the metal ion in transition states might be significantly different from that

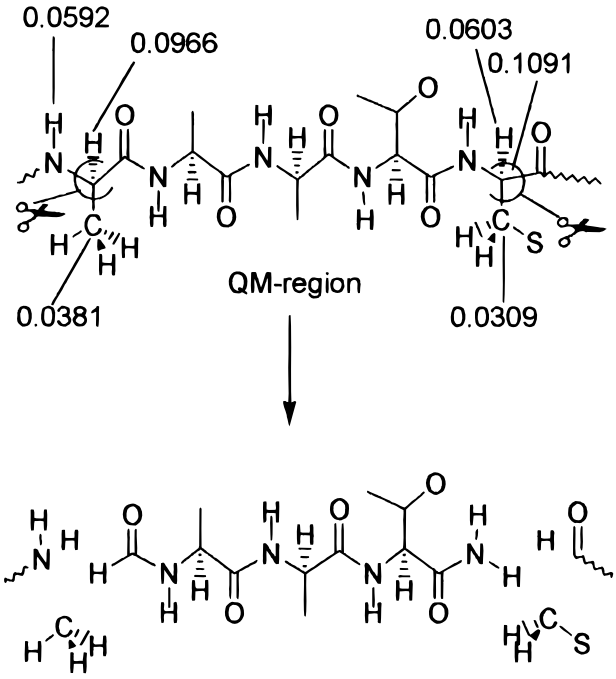

Figure 4. Schematic representation of the separation procedure to define the parts of the system treated quantum- and molecular-mechanically. The numbers indicate the Gasteiger−Marsili charges on the β-carbon, the amide hydrogen and the α-hydrogen of each residue at the separation border.

observed in the X-ray structure of the free enzyme or enzyme−inhibitor complexes. Thus, not only size and charge of the metal ion are decisive for catalytic activity, but also its preferred coordination geometry.[53]

Semiempirical calculations on simplified active site models suggest the formation of the tetrahedral intermediate to be rate-determining.[25] The results support the "catalytic triad" mechanism. Asp99 has a strong influence on the activation barrier of this step, as shown by model systems with and without this residue.[60] Because of the hydrogen bond network, which connects Asp99 with the N terminus, a further stabilizing effect on the energies and geometries, especially on structures with a positively charged His48, can be expected. Therefore, the approach of using a classical environment to investigate the electrostatic effects of the protein bulk on the active site promises a further insight into the catalytic mechanism and perhaps allows an indication favoring one of the two proposed mechanisms.

Methods

To perform the QM/MM calculations on a protein, it must be separated into quantum-mechanical (QM) and molecular-mechanical (MM) parts. The active site with the inhibitor or substrate treated quantum-mechanically must be separated from the protein bulk and saturated with hydrogen atoms. For this purpose the peptide chain is cut between the α-carbon and the amido nitrogen or the carbonyl carbon, respectively, of the first residue outside the QM part (Figure 4). The α-carbon is replaced by a hydrogen atom, forming terminating aldehyde or amino groups, respectively. The fragments of the "destroyed" residue remain in the classical part. In this way, the peptide fragment of the QM part contains, beside the active site residues, an aldehyde group and an amino group ensuring a closed shell QM system. To compensate the missing steric interactions of the QM atoms with the peptide chain, the backbone atoms of the

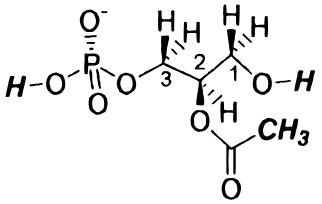

Figure 5. Simplified substrate structure used in the model systems **2**−**4**. The acyl group in the sn-1 position is substituted by a hydrogen, the sn-2 alkyl group is abstracted by a methyl group, and the sn-3 trimethylethylamino group replaced by a hydrogen. The simplified substituents are marked in bold, italic letters.

fragment in the QM part are slightly fixed by weak harmonic constraints with force constants between 5 and 20 kcal mol^{-1} Å^{-2} (for comparison: the force constant of a $C_{sp3} - C_{sp3}$ bond stretching potential is, according to the MM2 force field,[61] 317 kcal mol^{-1} Å^{-2}). The rest of the protein comprises fixed atom-centered point-charges (Gasteiger−Marsili)[62] with associated van der Waals potentials taken from the AMBER force field (PARM94)[63] implemented within VAMP 7.0.[64] The Coulombic interactions between the QM and the classical parts can be controlled by varying the dielectric constant ϵ. The geometry of the MM part was held frozen at the X-ray structure without prior relaxation, although X-ray structures may be strained. However, the active site residues including the side chains of the calcium-binding loop are calculated explicitly quantum-mechanically and therefore, are allowed to relax. The effect of the bulk of the enzyme on the active site is mainly electrostatic and the induced dipole moment depends more on the entire charge distribution than on the exact location of the individual charges. Only if allosteric interactions occur during the enzyme reaction is this method not appropriate. However, such interactions have not been observed in PLA_2.[44]

In the case of PLA_2, the QM part contains the Ca^{2+} ion, the simplified inhibitor, or substrate (Figure 5), and three peptide fragments of the active site: the calcium-binding loop (Tyr28, Cys29, Gly30, Arg31, and Gly32), His48, Asp49, and the catalytically important Asp99.

All calculations were performed with the semiempirical MO program VAMP 7.0[64] using the PM3 Hamiltonian[65] and the calcium parameters of Hehre and Wu.[66] For reaction paths and grid calculations in Cartesian coordinates, harmonic constraints were used to keep the distance between two atoms fixed. Here a force constant of 1000 kcal mol^{-1} Å^{-2} was used. Transition states were characterized by calculating the normal vibrations of the complete system. Because of the harmonic potentials used to constrain the atoms of the backbone to the positions of the X-ray structure, rotations, and translations may have low negative frequencies. However, in most cases these are about 1 order of magnitude smaller than the frequency corresponding to the reaction coordinate.

Validation of the QM/MM Separation

To investigate the influence of the separation procedure described above on the geometry, we used the X-ray structure of a human synovial fluid PLA_2 (PDB entry 1bbc)[67] as a test system and separated a tripeptide fragment. This X-ray structure was chosen because it is a monomer, has a high degree of secondary structure (about 60%), and contains no metal ions or solvent molecules. The separated peptide fragment (Ala102−Ala103−Thr104) (Figure 4) is part of an α-helix.

To gain information on the contributions of the point-charge environment and the harmonic constraints to a possible change in geometry compared to the X-ray structure, the tripeptide

TABLE 1: Conditions and RMS Deviation in Å for the Validation Systems a − d

system	point charge environment	harmonic constraints	RMS deviation
a	yes	yes	0.448
b	no	yes	0.158
c	yes	no	0.650
d	no	no	0.423

fragment was calculated four times with varying conditions, denoted as systems **a**−**d**. The systems were geometry optimized to a gradient norm of 0.1 kcal mol^{-1} $Å^{-1}$ using the PM3 Hamiltonian.[65]

In system **a** the fragment was optimized with weak harmonic constraints within the classical environment of the whole peptide. The force constants were 20 kcal mol^{-1} $Å^{-2}$ for amido nitrogen and carbonyl carbon atoms and, to keep the constraints on the side chains as small as possible, 10 kcal mol^{-1} $Å^{-2}$ for α-carbons. Further optimizations were carried out with harmonic constraints only (system **b**), classical environment only (system **c**), and without constraints or environment (system **d**). For each optimized structure the rms deviation relative to the X-ray structure for the heavy atoms was calculated. A survey of the conditions and results is given in Table 1.

Although in system **d** the optimization is unconstrained, the geometry of the X-ray structure was conserved well. The classical environment in system **c** has a slight influence on the geometry because of repulsive van der Waals interactions in the separation region. This effect can be compensated by the use of harmonic constraints, as shown in system **a**. Comparison with system **b**, which was optimized without the classical environment, shows that the force constants used are adequate to conserve the geometry.

The separation procedure suggested above in combination with the harmonic constraint technique can simulate the peptide environment for the quantum-mechanical treatment of an enzyme's active site. Furthermore, the Gasteiger−Marsili charges on the saturating hydrogen atoms and the β-carbon atoms (Figure 4) are below 0.1, so no significant electrostatic distortion is expected from the separation procedure.

The Model Systems

To investigate the reaction mechanism considering environmental effects to varying degrees, four different model systems with increasing QM size were created. The largest of them was treated additionally with a classical environment. The minimal model (system **1**) contains imidazole to represent His48, methyl acetate, and water as reactants. No metal center is present. An extended system (**2**) is formed by a Ca^{2+} ion, a pentaglycine fragment abstracting the calcium-binding loop, the bidentate Asp49, His48 and sn-glycero-2-acetyl-3-phosphate (Figure 5) as substrate. System **3** additionally contains Asp99, which forms a hydrogen bond to the nitrogen Nϵ2 of His48 (Figure 1). The active site model (system **4**) contains the fragment used in system **3**, but here the calcium-binding loop is built using the residues Tyr28, Cys29, Gly30, Arg31, and Gly32. The termini of all chain fragments are treated as described above. Furthermore, system **4** has been calculated within a classical environment representing the rest of the enzyme.

The influence of the dielectric constants for the polarizing effect of the classical environment on the quantum-mechanical system was additionally investigated by a series of calculations on system **4** with dielectric constants for the protein environment varying between $\epsilon = 1$ and $\epsilon = 78$.

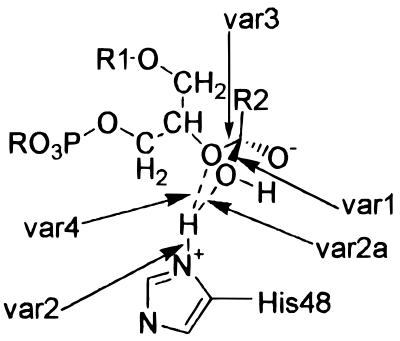

Figure 6. Variables used for the grid calculations on the systems **2**−**4**. Only distances are changed.

Results and Discussion

The Active Site Model without Protein Environment. In our earlier studies we performed grid calculations for the ester hydrolysis for the systems **1**, **2**, and **3**.[25,60] The results show that in system **1** the reaction between imidazole, methyl acetate, and water occurs in two steps. First the tetrahedral intermediate is formed by the deprotonation of the water molecule by imidazole and the nucleophilic attack on the carbonyl oxygen as a concerted process. The transition state for this step has one imaginary vibration with a frequency of −2253 cm^{-1}. The activation barrier amounts to 43.0 kcal mol^{-1}. Subsequently the tetrahedral intermediate collapses under the cleavage of the bond between the carbonyl carbon and the ester oxygen and the protonation of the methanolate ion by imidazole. This step passes a transition state with a very soft imaginary vibration (frequency of −253 cm^{-1}) that corresponds to an alcoholate structure. The bond between the carbonyl carbon and the ester oxygen is already broken, but the protonation of the ester oxygen has not yet occurred. The decomposition reaction cannot be described by a single reaction coordinate, but rather by two − the distance between the carbonyl carbon and the ester oxygen and the distance between the ester oxygen and the hydrogen.

For the grid calculations for systems **2** and **3** the variables for the first step (Figure 6) were the distances between the carbonyl carbon of the sn-2 ester group of the substrate (var1) and the nucleophilic water oxygen and between the nitrogen Nδ1 of His48 and the water hydrogen (var2). The second step variables were the distances between the carbonyl carbon and the ester oxygen (var3) and between the ester oxygen and the hydrogen which is bound to the nitrogen Nδ1 of His48 (var4). The resulting energy surfaces indicate strongly that the first step follows a path similar to that found for system **1**. In both systems **2** and **3**, the water deprotonation and the nucleophilic attack form a concerted process over a single transition state. Frequencies for the imaginary vibrations of −2327 cm^{-1} for system **2** and −2065 cm^{-1} for system **3** were found. The activation barrier of system **2** (27.8 kcal mol^{-1}) is considerably lower than that of the minimal system **1** and even lower in system **3** (20.6 kcal mol^{-1}).

In a second step the ester bond of the tetrahedral intermediate is cleaved and an alcoholate structure results. The activation energy for the bond cleavage amounts to 12.3 kcal mol^{-1} in system **2** and to 9.7 kcal mol^{-1} in system **3**; the frequency of imaginary vibration belonging to the transition state is −136 cm^{-1} (system **2**) and −226 cm^{-1} (system **3**). The relative energy of the alcoholate structure is 15.3 kcal mol^{-1} in system **2** and 5.6 kcal mol^{-1} in system **3**. Finally, as a third step of the hydrolysis reaction, the alcoholate is protonated with an activation barrier of 3.7 kcal mol^{-1} (frequency −1820 cm^{-1}) in system **2** or 1.7 kcal mol^{-1} (frequency −2184 cm^{-1}) in system

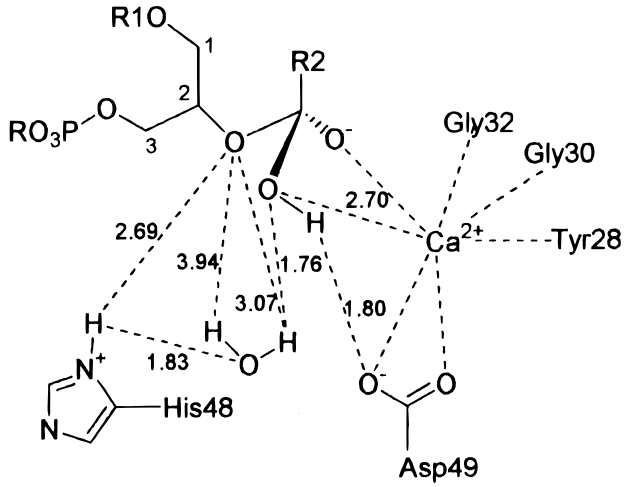

Figure 7. Schematic representation of the geometry of the active site (tetrahedral intermediate) containing two water molecules. The dashed lines indicate important interatomic distances in Å.

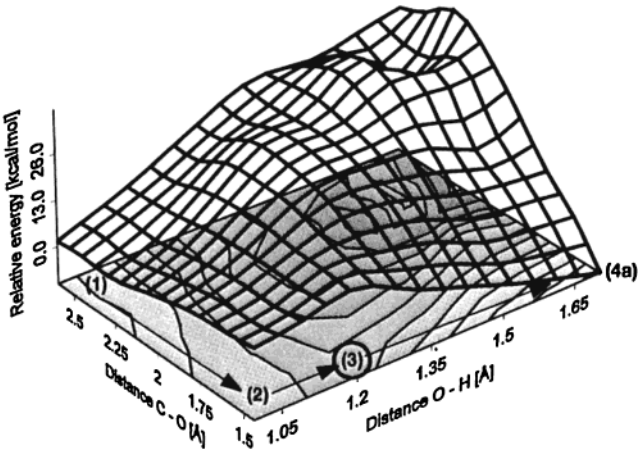

Figure 8. Energy surface for the formation of the tetrahedral intermediate in system **4**; see Figure 10 for the numbering of the structures.

3. Except for the differences of the relative energies the reaction path of systems **2** and **3** is similar.[25,60]

The calculations for these systems suggest clearly that the formation of the tetrahedral intermediate is the rate-limiting step and, thus, support the "catalytic triad" mechanism.

The Active Site Model within Protein Environment. To investigate the influence of the protein environment on the enzymatic reaction, grid calculations similar to those performed for systems **2** and **3** were carried out. For this purpose the active site model containing the side chains of the calcium-binding loop was placed within a point-charge environment forming system **4**.

The dielectric constant ϵ inside a protein depends on the specific site.[68] In the case of trypsin, King et al. found ϵ values between 3 and 20 for different regions using microscopic simulation methods on solvated proteins.[69] In the electrostatic model used in this work a homogeneous ϵ for the protein bulk is assumed. This approximation is reasonable because the major part of the active site is calculated explicitly. However, which ϵ value is appropriate to describe the electrostatic effects of the protein environment on the active site? Based on the conclusions reached by King et al., a dielectric constant $\epsilon = 4$ for system **4** should be realistic.

First we investigated whether a second water molecule that deprotonates the nucleophilic water molecule is present in the active site, as proposed in the literature.[42,50,52,53] Therefore, the active sites of the free enzyme, the educt complex, and the tetrahedral intermediate of system **4** were extended by an additional water molecule followed by geometry optimization. In the starting geometries the additional water molecule was located in a hydrogen-bonding position between His48 and the equatorial water molecule in the free enzyme, and between the nucleophilic water in the educt complex or the OH-group of the tetrahedral intermediate. During optimization the water molecule moves toward the protein environment. In the case of the tetrahedral intermediate, it retains a hydrogen bond to Nδ1 of His48 and the OH-group of the substrate, but moves markedly away from the connecting line between Nδ1 and the OH-group away from the ester oxygen. The structure is shown schematically in Figure 7. The distance between the hydrogen atom of the additional water molecule, which is not involved in the hydrogen bonding pattern and is proposed to protonate the ester oxygen during the decomposition step, and the ester oxygen is 3.94 Å. In comparison, the hydrogen bonded to Nδ1 is only 2.69 Å away from the ester oxygen. It is thus more likely that the proton transfer in the decomposition step occurs between His48 and the ester oxygen. The situation in the educt complex is similar, the additional water does not remain near its starting position. Even in the free enzyme it is not located in a position on the connecting line between His48 and the equatorial water, but moves in the same direction as in the enzyme−substrate complex. Obviously the conformation of the active site is more favorable if only one water molecule is present. Especially, the conditions for the decomposition step, which is proposed to be rate-limiting in the "oxyanion" mechanism, are less favorable if the active site contains an additional water.

However, is a second water molecule additional to the nucleophilic water really necessary allow the formation of a calcium-coordinated hydroxide ion as the "oxyanion" mechanism requires? The second water has been invoked in the catalytic mechanism because, according to crystal structures, the distance between a calcium-coordinated nucleophilic water molecule and Nδ1 of His48 seems to be too large to allow a proton transfer to form a calcium-coordinated hydroxide ion.[42] The distance between the calcium ion and Nδ1 of His48 in the crystal structure determined by Thunnissen et al.[47] is 6.48 Å. Our calculations and MD-simulations,[41] however, have shown that the active site geometry can change significantly without undergoing large conformational changes. The geometry-optimized educt−enzyme complex exhibits a calcium-coordinated water molecule (the $Ca^{2+}-O_{H_2O}$ distance is 2.71 Å) and a hydrogen bond between Nδ1 of His48 and the water hydrogen with a length of 1.79 Å. Therefore, calcium coordination of the nucleophilic water and simultaneous hydrogen bonding to His48 are possible. Furthermore, no water molecule is present within the active site in X-ray structures of enzyme−inhibitor complexes.[46,47] Taking these results into account, we performed grid calculations on the active site model containing the active site with only the nucleophilic water in a classical environment with $\epsilon = 4$ (system **4**). The variables chosen are shown in Figure 6.

A comparison with our results obtained for system **3**[25,60] reveals a different reaction path for formation of the tetrahedral intermediate. Although a transition state for this step was found in system **3**, the energy hypersurface for system **4** (Figure 8) shows that first the water molecule is added to the substrate, forming a bond between the water oxygen and the carbonyl carbon, and then the proton transfer to His48 takes place. The reaction path describing the addition of the water molecule to

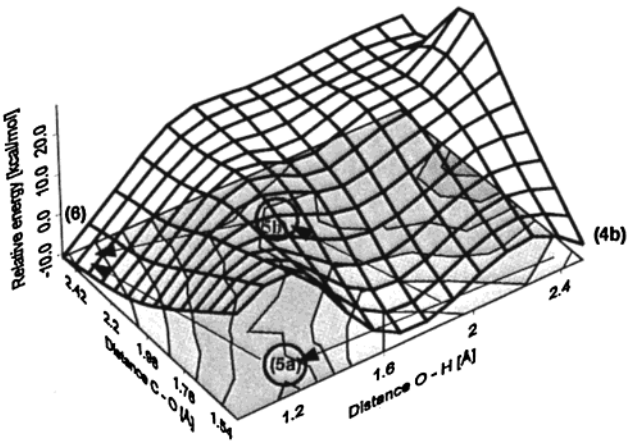

Figure 9. Energy surface for the decomposition of the tetrahedral intermediate in system **4**; see Figure 10 for the numbering of the structures.

the carbonyl carbon (var1 as variable) shows that the transition state lies very close to the substrate−water adduct. The activation energy for this step amounts to 8.3 kcal mol^{-1} and the relative energy of the substrate−water adduct to 8.2 kcal mol^{-1}. However, the characterization of the transition state in this system is difficult because of the use of harmonic constraints. The negative frequency characterizing the water addition is in the same range as the "artificial" frequencies. In a small model system, the addition of a water molecule to methyl-acetate protonated at the carbonyl oxygen the transition state has been determined and characterized by force and *intrinsic reaction coordinate* (IRC) calculations. The frequency of the imaginary vibration is -304 cm^{-1}, and visualization of the vectors shows that the frequency belongs to a combination of several vibrations. The difference between the transition state energy and the relative energy of the product here is also only very small (1.1 kcal mol^{-1}). However, this step is of minor importance, because it is clearly not rate-limiting. Actually, this mechanism step shows more similarity to an acid-catalyzed ester hydrolysis than to the general base catalysis mechanism involving the formation of a hydroxide ion.

The reaction path (var2a as variable) of the subsequent proton transfer passes a transition state with a relative energy of 13.7 kcal mol^{-1}. The activation barrier of this step is 5.5 kcal mol^{-1}. The calculated frequency of the imaginary vibration is -2014 cm^{-1}.

The grid calculation of the decomposition step (variables var3 and var4 shown in Figure 6; energy surface shown in Figure 9) again shows another reaction path for system **4** than for system **3**. Whereas this step in the smaller system **3** clearly takes place in two parts, it is concerted in system **4**. The energy surface reveals two alternative saddle points with different geometries, but energies only 1.3 kcal mol^{-1} apart. The energetically more favorable path passes a transition state (Figure 10, structure 5b) with a relative energy of 15.6 kcal mol^{-1}. Here the bond cleavage between the carbonyl carbon and the ester oxygen is already complete and the protein transfer is still in progress. The ester oxygen is coordinated to the calcium ion at a distance of 2.68 Å. The imaginary vibration has a calculated frequency of -2240 cm^{-1}. The activation barrier for this step is 22.7 kcal mol^{-1}.

In the alternative transition state (structure 5a in Figure 10; relative energy 16.9 kcal mol^{-1}; negative frequency -2319 cm^{-1}) the bond between the carbonyl carbon and the ester oxygen is slightly lengthened to a distance of 1.56 Å, but not yet broken. The proton transfer step is not as advanced as in the transition state structure 5b described above. Here the distance between the ester oxygen and the calcium ion amounts to 3.18 Å. The activation barrier is 24.0 kcal mol^{-1}.

The geometries of the structures obtained are given in Figure 10; relevant distances are shown in Table 2. Figure 11 shows the energy profile of the reaction path obtained by the QM/MM calculations with a dielectric constant $\epsilon = 4$.

In contrast to our earlier results obtained for systems **2** and **3**, the calculations for system **4** clearly suggest that the rate-limiting step is the decomposition of the tetrahedral intermediate. Thus, the result supports the "oxyanion" mechanism.

Changes of the Coordination Number of the Calcium Ion During the Reaction and Flexibility of the System. During the reaction the coordination number of the calcium ion changes several times, and several nearly equivalent structures with different calcium-coordination numbers have been obtained. The changes in coordination number are accompanied by conformational changes of Asp49, which flips the plane of its carboxylate group by about 50 degrees when the calcium ion is coordinated by eight ligands relative to a coordination number of seven.

In the educt complex (structure 1 in Figure 10) the metal ion has a coordination number of eight − the three ligands of the calcium-binding loop, the bidentate Asp49, the polar headgroup, and the carbonyl oxygen of the substrate and the nucleophilic water molecule, which has a distance to the calcium ion of 2.71 Å. This distance increases to 3.63 Å during the formation of the tetrahedral intermediate (structure 4a) and decreases again during the decomposition step. It amounts to 2.50 Å in the transition state structure (structure 5a) and to 2.55 Å in the

TABLE 2: Relevant Distances of the Stationary Points Obtained by Grid Calculations on System 4 ($\epsilon = 4$) in Å (see Figure 10)

structure	1	2	3	4a	4b	5a	5b	6a	6b
distance between									
$Ca^{2+}-O_{CO}$ (Tyr28)	2.42	2.38	3.37	2.36	2.41	2.40	2.50	2.49	2.48
$Ca^{2+}-O_{CO}$ (Gly30)	2.55	2.44	2.44	2.42	2.52	2.49	2.53	2.48	2.49
$Ca^{2+}-O_{CO}$ (Gly32)	2.57	2.41	2.50	2.50	2.59	2.61	2.88	2.79	2.76
$Ca^{2+}-O\delta1$ (Asp49)	2.50	2.44	2.47	2.46	2.61	2.59	2.51	2.52	2.53
$Ca^{2+}-O\delta2$ (Asp49)	2.51	2.47	2.49	2.49	2.42	2.43	2.45	2.44	2.44
$Ca^{2+}-O_{headgroup}$ (substr.)	2.27	2.26	2.26	2.27	2.28	2.31	2.33	2.34	2.33
$Ca^{2+}-O_{CO}$ (substr.)	2.41	2.30	2.29	2.28	2.29	2.45	2.61	2.73	2.65
$Ca^{2+}-O_{ester}$ (substr.)	4.04	3.92	3.98	3.91	3.86	3.18	2.68	2.69	2.69
$Ca^{2+}-O_{wat}$ or O_{OH} (substr.)	2.71	3.12	3.38	3.63	2.74	2.50	2.61	2.55	2.57
C_{CO} (substr.)$-O_{wat}$	2.57	1.58	1.47	1.41	1.42	1.39	1.34	1.34	1.34
C_{CO} (substr.)$-O_{ester}$ (substr.)	1.34	1.39	1.42	1.45	1.43	1.56	2.34	2.49	2.47
$N\delta1$ (His48)$-O_{ester}$ (substr.)	3.46	3.38	3.41	3.15	3.12	2.58	2.64	2.83	2.84
$H_{water}-N\delta1$ (His48)	1.79	1.68	1.30	1.02	1.02	1.35	1.28	1.86	1.85
$H_{water}-O_{ester}$ (substr.)	3.00	2.39	2.55	2.45	2.48	1.24	1.38	0.98	0.98
$H_{N\epsilon2}$ (His48)$-O\delta1$ (Asp99)	1.73	1.71	1.69	1.67	1.67	1.67	1.68	1.70	1.70

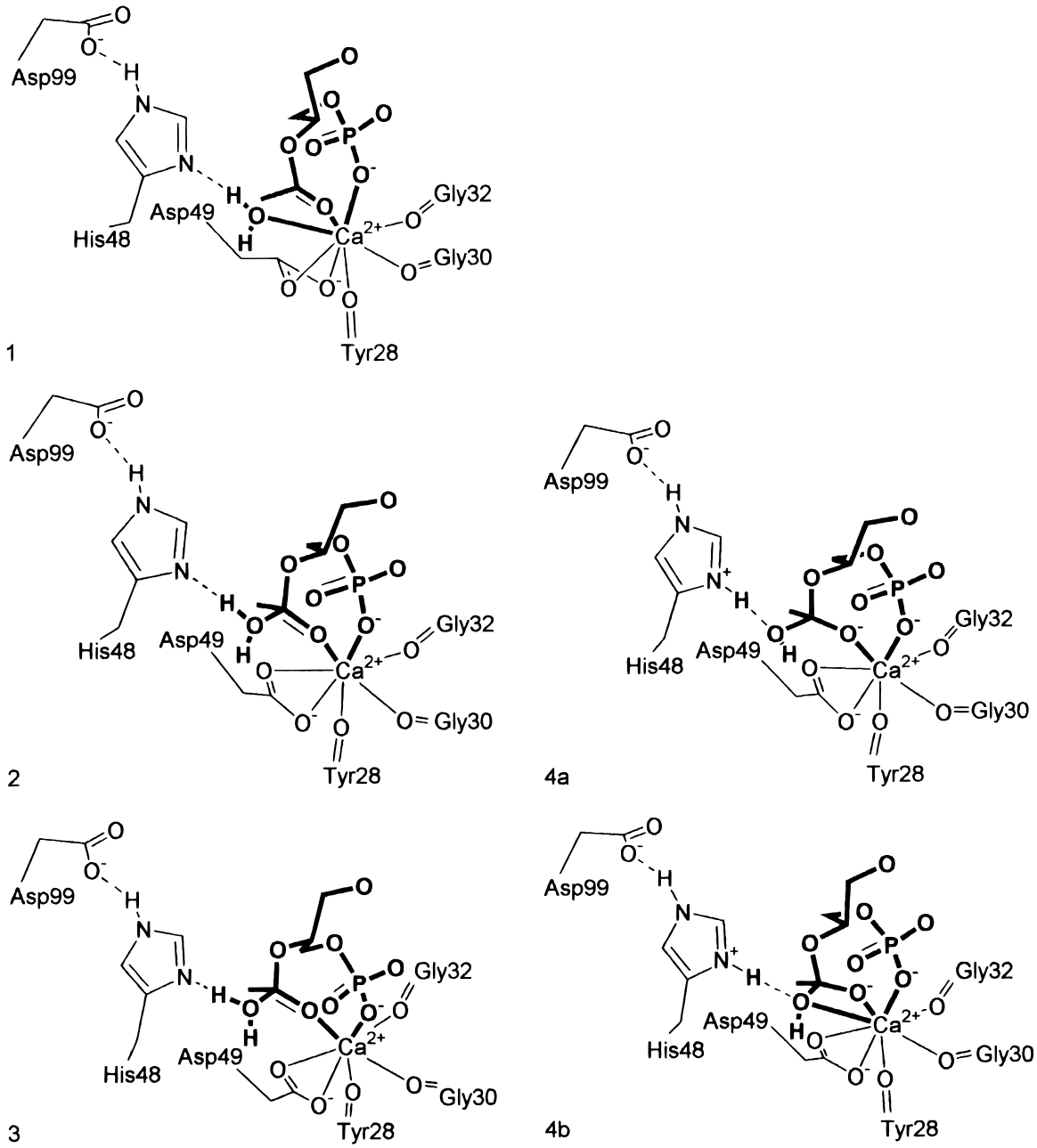

Figure 10. Two-dimensional projection of the geometries of the stationary points obtained from the grid calculations on system **4**; the substrate and the nucleophilic water are marked bold. The educt complex (structure 1), the substrate−water adduct (structure 2), and the transition state structure of the formation of the tetrahedral intermediate (structure 3). Two different structures of the tetrahedral intermediate with different coordination numbers of the Ca^{2+} ion: in structure 4a the coordination number is seven, in structure 4b it is eight because of the calcium-coordinated hydroxyl group. Two different structures of the transition state for the deformation step of the tetrahedral intermediate. In structure 5a the bond between the carbonyl carbon and the ester oxygen is not yet broken (coordination number of the Ca^{2+} ion is eight); in structure 5b the cleavage is almost complete, the coordination number is nine because of the calcium-coordinated ester oxygen. Structure 6 shows the product complex.

product complex (structure 6a). The coordination number of the tetrahedral intermediate is seven, but another minimum has been found (structure 4b), where the distance between the calcium ion and the oxygen is 2.74 Å and which has a relative energy of −7.1 kcal mol^{-1}, compared to −9.4 kcal mol^{-1} for the first structure. Here the coordination number is eight.

The decomposition step is stabilized by the coordination of the ester oxygen as soon as the bond between the carbonyl carbon and the ester oxygen is broken. The two transition state structures (5a and 5b) for the decomposition step show a correlation between the bond cleavage and the calcium coordination of the ester oxygen. The more the bond cleavage between the carbonyl carbon and the ester oxygen is advanced, the more the ester oxygen is coordinated to the calcium ion, to stabilize the negatively charged oxygen atom.

The product complex (structure 6) has a coordination number of nine. However, again another very similar minimum (6b) has been detected (the rms deviation for all atoms including hydrogen atoms is 0.086 Å) and has a relative energy of −9.7 kcal mol^{-1}, compared to −10.8 kcal mol^{-1}.

These considerations support the suggestion of Yu et al.[59] that the coordination behavior of the calcium ion makes an important contribution to its function during the enzymatic reaction and, thus, again indicates the "oxyanion" mechanism. Furthermore, the fact that for the structures 4, 5, and 6 several minima have been obtained that differ slightly in their relative

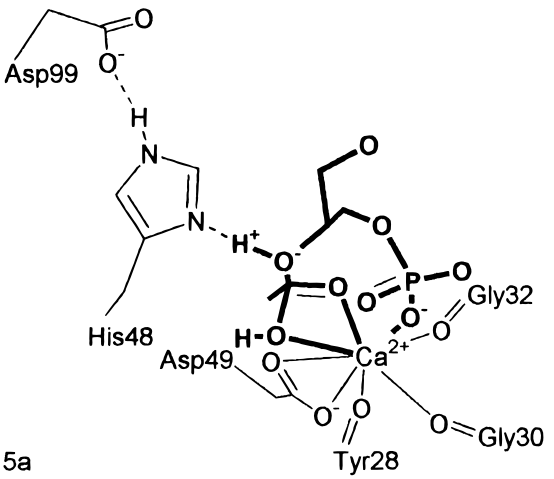

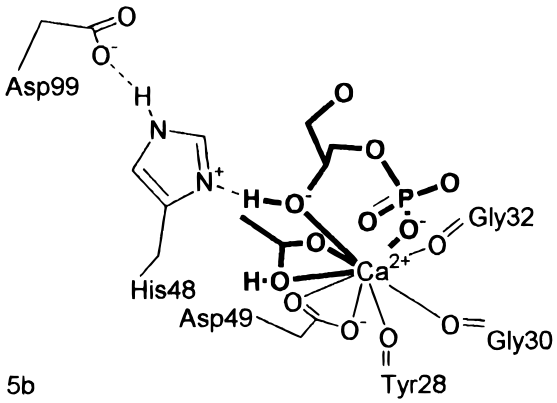

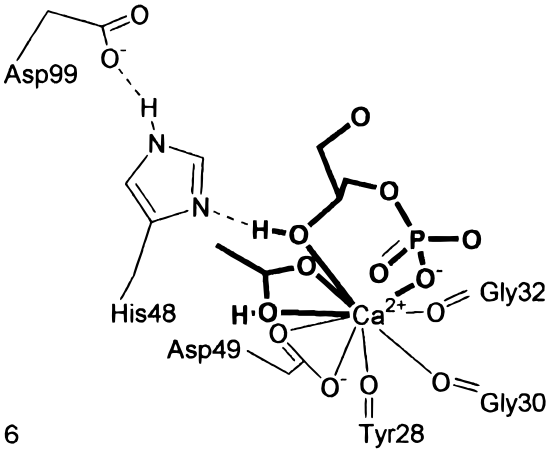

energies and, in the case of structures 4 and 5, even in the coordination number of the calcium ion, confirms the flexibility of the active site, as observed by Jones et al.[41]

Influence of the Dielectric Constant ϵ on the Calculated Energies. A comparison between our calculations of the ester hydrolysis including only the enzyme active site and those that take the protein environment into account shows that the environmental effect largely determines the course of the reaction. For the grid calculations on system **4** a dielectric constant of $\epsilon = 4$ was used. To investigate the influence of the protein environment further, we reoptimized the system with dielectric constants varying from $\epsilon = 1$ to $\epsilon = 78$. To allow a comparison to systems **1**−**3**, the structures obtained as stationary points in system **3** were chosen for the recalculations as starting points. For clarity, the structures are numbered as following: I is the educt complex, II the transition state for the formation step of the tetrahedral intermediate, III the tetrahedral intermediate, IV the alcoholate structure, and V the product complex. The ester−water adduct (structure 2 in Figure 10) has been ignored, because there is no corresponding structure in systems **2** and **3** and the geometry of the alcoholate structure obtained from the calculations on systems **2** and **3** was extended with the side chains of the calcium-binding loop and the protein environment.

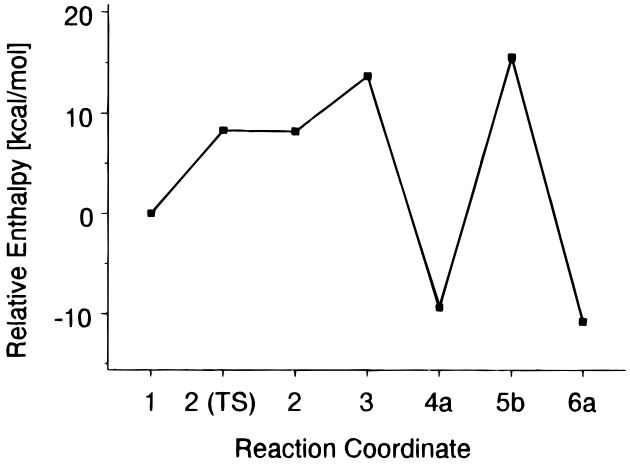

Figure 11. Energy profile of the reaction path of the catalyzed ester hydrolysis (system **4**); see Figure 10 for the numbering of the structures.

To show the effect of the Coulombic interaction on the stability of each structure, the calculations were performed with different dielectric constants, ϵ between 1, in a vacuum, and 78, corresponding to water, forming the systems $\mathbf{4_1}$ ($\epsilon = 1$), $\mathbf{4_2}$ ($\epsilon = 2$), $\mathbf{4_4}$ ($\epsilon = 4$), $\mathbf{4_8}$ ($\epsilon = 8$), and $\mathbf{4_{78}}$ ($\epsilon = 78$). For comparison purposes system **4** was also recalculated without the protein environment (system $\mathbf{4_0}$). In system $\mathbf{4_{78}}$ ($\epsilon = 78$) the Coulombic interaction between the active site and the protein bulk is almost turned off and the energy contribution to the heat of formation is smaller than 1 kcal mol^{-1}. However, a considerable influence on the relative energies of the geometries investigated results from the van der Waals interactions with the protein environment.

Figure 12 shows that the energy profiles of the different systems depend strongly on the environment used. While the relative energies of the uncharged products (structure V) differ over a range of about 10 kcal mol^{-1}, the energy range of the tetrahedral intermediates (structure III) is about 50 kcal mol^{-1}. Because of the charge separation in the tetrahedral intermediate, the stabilization by the environment is much more evident. A similar effect can be observed for the transition state of the first step (structure II) and for the alcoholate (structure IV). A detailed list of the relative energies is given in Table 3.

In the minimal system **1**, the tetrahedral intermediate (structure III) that shows a formal charge separation caused by the proton transfer can only be stabilized by a specific arrangement of the components. This means that a hydrogen bond between the protonated imidazole and the tetrahedral intermediate must be formed. In the extended system **2**, the charged calcium ion (the calculated Coulson charge using the PM3 Hamiltonian is 1.12) allows a further stabilization of the coordinated tetrahedral intermediate. In system **3** a strong lowering of the relative energy is caused by the presence of Asp99, which additionally stabilizes the positive charge on His48. A further stabilization can be observed in the systems $\mathbf{4_{78}}$ to $\mathbf{4_0}$. The active site model, even without the enzyme environment (system $\mathbf{4_0}$), has a 1.8 kcal mol^{-1} lower energy than the tetrahedral intermediate in system **3**, which can be explained by the better stabilization of the negatively charged substrate via hydrogen bonds to the amide

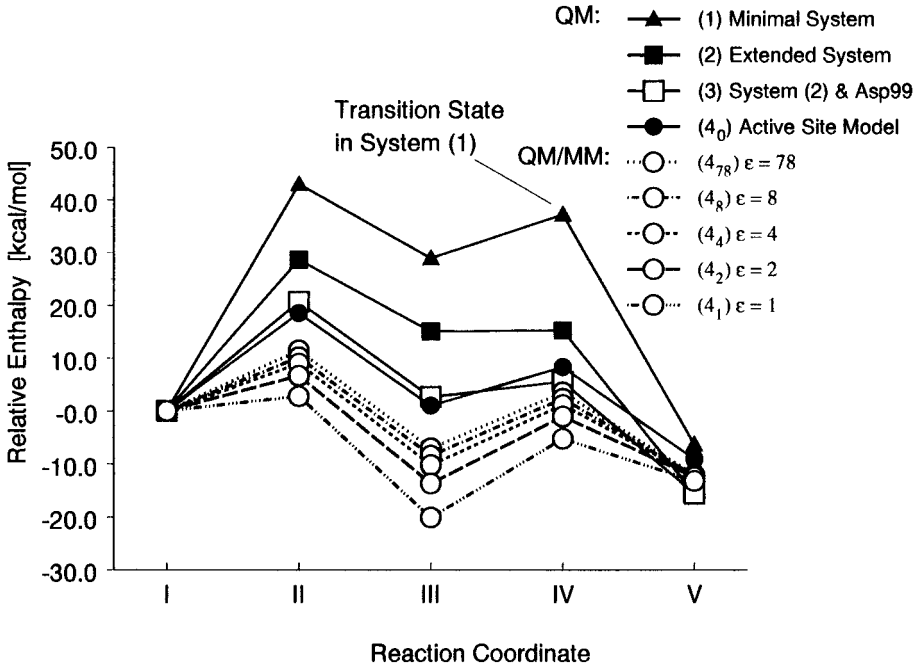

Figure 12. Energy profiles for the model systems **1**−**3**, **4$_0$**, and **4$_{78}$**−**4$_1$**: I is the educt complex, II the transition state for the formation step of the tetrahedral intermediate, III the tetrahedral intermediate, IV the alcoholate structure, and V the product complex.

TABLE 3: Relative Energies of the Model Systems 1−4 in kcal mol^{-1}; the Alcoholate Structure IV of System 1 Is a Transition State

system	1	2	3	4$_0$	**4$_{78}$** ($\epsilon = 78$)	**4$_8$** ($\epsilon = 8$)	**4$_4$** ($\epsilon = 4$)	**4$_2$** ($\epsilon = 2$)	**4$_1$** ($\epsilon = 1$)
structure									
I	0	0	0	0	0	0	0	0	0
II	43.0	28.7	20.7	18.6	11.5	10.2	9.0	6.7	2.8
III	29.0	15.1	2.7	1.0	−7.0	−8.4	−10.2	−13.7	−20.1
IV	(36.0)	15.3	5.6	8.4	3.6	2.4	1.2	−1.0	−5.2
V	−6.3	−15.6	−15.6	−9.1	−12.1	−12.3	−12.1	−12.4	−13.2

nitrogen atoms of Gly30 and Gly32, because charge can be delocalized to the side chains of the calcium-binding loop. Asp99 connects the active site with the N terminus of the protein via a hydrogen bond network. In this way the electrostatic effect of Asp99 is increased. This effect is most distinct with $\epsilon = 1$. However, even with $\epsilon = 78$ in system **4$_{78}$**, where the Coulombic interaction is almost shielded, the relative energy is lowered by about 8 kcal mol^{-1} compared to system **4$_0$**. This stabilization is mostly due to favorable van der Waals interactions of the active site with the environment.

The enzyme environment also causes a considerable lowering of the activation barrier of the first reaction step. Compared to system **4$_0$**, which has an activation energy of 18.5 kcal mol^{-1}, the relative energy of the transition state (structure II) in system **4$_{78}$** is lowered by 7 kcal mol^{-1}. In system **4$_1$**, where the active site is not shielded from electrostatic effects, the activation energy decreases to only 3 kcal mol^{-1}.

The alcoholate structure (structure IV) also shows a charge separation and, therefore, a stabilization can be expected in systems **4$_{78}$** to **4$_1$**. However, this effect is not as large as expected. The difference between systems **4$_0$** and **4$_{78}$** is about 5 kcal mol^{-1}. In system **4$_1$** the decrease in the relative energy amounts to 10 kcal mol^{-1}. Interestingly, the relative energy for the alcoholate structure in system **4$_0$** is almost 3 kcal mol^{-1} higher than in system **3**. On one hand, this is because the flexible side chains of the active site model system **4** can undergo large conformational changes in the absence of the enzyme environment. On the other hand, the effect of the calcium-binding loop side chains on the active site has a strong influence on the electrostatic environment of the substrate and, thus, on the stabilization of intermediates. However, this alcoholate structure, although a minimum, is not involved in the reaction, as reflected by its high relative energy.

For the uncharged product structure (structure V) there are no significant differences in the relative energies in the systems **4$_{78}$** to **4$_1$**; the classical environment causes a decrease of about 3 to 4 kcal mol^{-1} in these systems compared to system **4$_0$**.

Clearly, the protein environment, represented by point charges, exerts a strong electrostatic influence on the active site. This can be demonstrated using the dipole moments of systems **4$_{78}$**−**4$_1$** compared to the dipole moment of system **4$_0$** for the transition state structure of the first reaction step (structure II). Not only the magnitude of the dipole moment vector increases continuously from 1.0 D in the case of system **4$_{78}$** to 13.4 D in system **4$_1$**, but it also rotates by 4° on inclusion of the environment ($\epsilon = 1$). The differences in the charge distribution can be visualized by superimposing structure II of system **4$_1$** and the corresponding structure calculated as a single-point in the gas phase (Figure 13). The subtraction of the electron densities represented as natural atomic orbital point charges (NAO-PCs)[70] of the superimposed structures from one another shows the differences in the charge distribution. The result of this procedure shows that the largest effect of the protein environment can be observed at the calcium-binding loop. These comparisons indicate that the protein bulk provides an exactly adjusted environment for the reaction catalyzed by the enzyme.

At this point a comparison with the ab initio QM/MM calculations of Waskowycz et al.[20] is appropriate. They used a static classical environment with a quantum-mechanical system consisting of methyl formate (as the substrate), β-methyl-

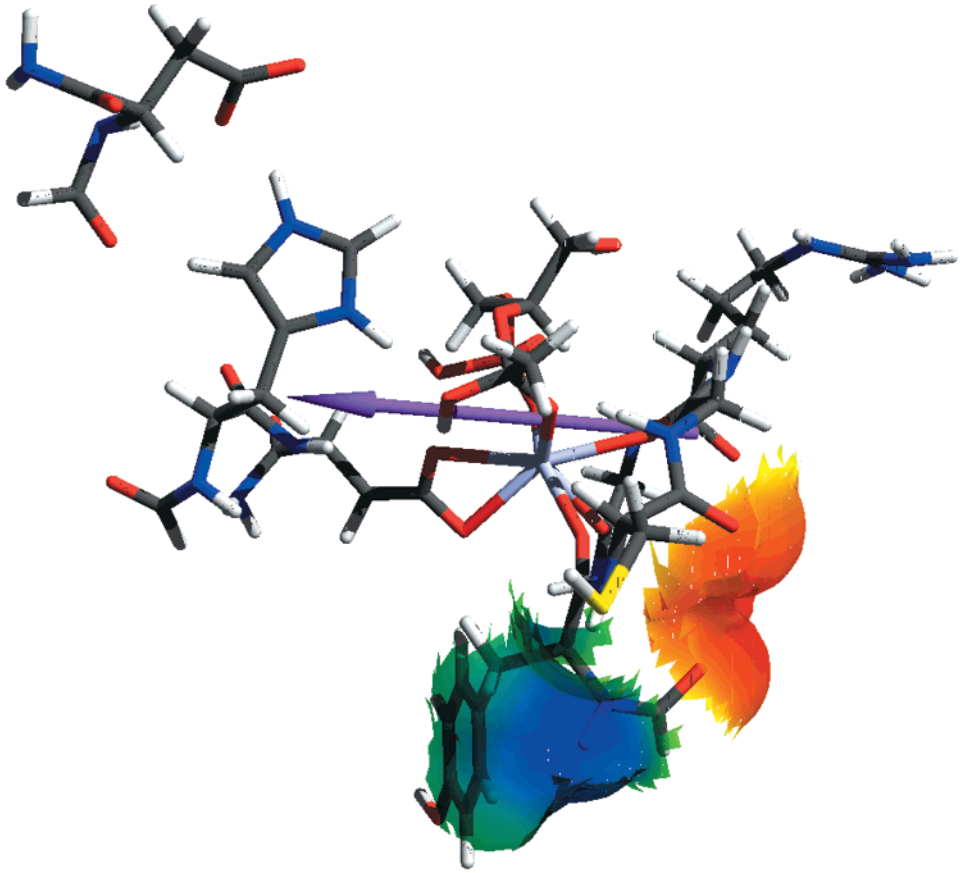

Figure 13. Superimposition of structure II calculated within the protein environment ($\epsilon = 1$) and the corresponding structure calculated in the gas phase. The differences in the charge distribution are mapped on the solvent excluded surface (SES). For clarity, only the extrema are shown by excluding the range between −25 and 40 kcal mol^{-1}. The resulting dipole moment vector (10 D) is represented by the arrow.

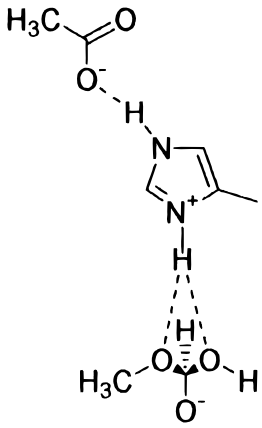

Figure 14. Model system used by Waskowycz et al. for the quantum-mechanical part within the QM/MM calculations on PLA_2.

imidazole (as His48), and acetate (as Asp99) (Figure 14). The imidazolium−oxyanion system was optimized at the HF/3-21G level. A series of optimized intermediate structures along the reaction surface was also generated using the C−OH bond of methyl formate as the reaction coordinate in order to model the surface toward the reactants and the C−OMe bond as the coordinate to model the formation of the products. Single-point calculations at the HF/4-31G level were performed for the structures obtained within the MM-environment (in situ) and in the gas phase (in vacuo). Because of the different substrates, a comparison of the geometry of the oxyanion system to the tetrahedral intermediate of system **4** ($\epsilon = 4$) can only be qualitative. The main difference lies in the position of the substrate relative to the imidazolium ion representing His48. The ab initio structure shows a distance between the hydrogen atom bonded to Nδ1 of His48 to the ester oxygen of 2.02 Å, compared to 2.45 Å in system **4**. The distance between the amide hydrogen of Gly30 and the carbonyl oxygen of the substrate is also 0.15 Å shorter in the tetrahedral intermediate of system **4**. In our calculations the substrate lies closer to the calcium-binding loop. The hydrogen bond between the ester oxygen and the imidazolium of His48, which is present in the ab initio structure, is therefore not found. However, this is probably a result of the missing polar headgroup when methyl formate is used to represent the substrate. This polar headgroup forms a hydrogen bond to the amide hydrogen of Gly32, which is not possible in the ab initio structure. In this way the position of the substrate is fixed to a certain degree.

The energy surfaces of the two different QM/MM calculations are also of interest, although, because of the different systems calculated, the energy profiles again can only be compared qualitatively. Nevertheless, our semiempirical results support those of Waskowycz et al. The ab initio in vacuo calculations show a large barrier for the formation of the oxyanion (about 20 kcal mol^{-1}) in comparison to the in situ model, which has a distinct minimum (about −12 kcal mol^{-1}) at the oxyanion structure. The stabilization of the tetrahedral intermediate by the electrostatic environment of the protein is found in both studies.

The relative energy profiles (Figure 12) show that the calculated reaction path depends on the environment and the dielectric constant. In the models **1**−$\mathbf{4_0}$, the first step is clearly rate-determining. For all systems the ratio between the activation barrier of the first step of the hydrolysis reaction and the energy difference between the tetrahedral intermediate and the alco-

holate structure are decreasing the more environmental effects are taken into account. This is because the tetrahedral intermediate is stabilized strongly by the environment. The QM/MM systems $\mathbf{4_{78}}$ to $\mathbf{4_1}$ show a change in the nature of the energy profile. While in system $\mathbf{4_{78}}$ ($\epsilon = 78$) the activation barrier and the energy difference between the tetrahedral intermediate and the alcoholate are almost equal, the ratio in system $\mathbf{4_1}$ ($\epsilon = 1$) is about 5.

Conclusions

The results obtained from our QM/MM calculations support the reaction mechanism proposed by Rogers et al.[50] The decomposition step of the tetrahedral intermediate becomes rate-limiting when the protein environment is taken into account. Furthermore, we have confirmed that the coordination behavior of the calcium ion allows the interaction with additional ligands. In this way the nucleophilic water is shifted inside the coordination shell of the metal ion. However, the presence of a second water molecule, also proposed by Rogers et al.,[42,50] which connects the nucleophilic water with nitrogen Nδ1 of His48 via hydrogen bonds, cannot be confirmed. A much more favorable conformation is a direct hydrogen bond between the nucleophilic water and His48. The same qualitative result has been obtained by molecular dynamics simulations.[41] The formation of a calcium-coordinated hydroxide ion is also not an energetically favorable process, as the grid calculations show (Figure 8). The oxygen of the nucleophilic water is first added to the carbonyl carbon and the proton transfer takes place in a second step.

Summarizing, a considerable flexibility of the active site and the substrate is found, as proposed previously in other papers.[41,53] Although no large conformational changes occur, the flexibility of the substrate and His48 allows the active site to move the ligands into different positions, where either a hydrogen bond between Nδ1 of His48 and the nucleophilic water, between Nδ1 and the hydroxyl-group of the tetrahedral intermediate or between Nδ1 and the ester oxygen, can be formed.

Although the reaction mechanism found is plausible, the activation barrier of the decomposition step is high (at least 22.7 kcal mol^{-1}). Using the Eyring equation

$$k = \frac{k_B T}{h} \times e^{-(\Delta G^*/RT)} \qquad (1)$$

(k is the rate constant, k_B the Boltzmann constant, T the absolute temperature (310 K), h the Planck constant, ΔG^* the activation energy and R the molar gas constant) a rate constant of 6.6×10^{-4} s^{-1} can be estimated, which is about 6 orders of magnitude lower than those found experimentally (675 s^{-1} for the hydrolysis of 1,2-dioctanoyl-*sn*-glycero-3-phosphocholine micelles,[71] which would correspond to an activation barrier of 14.2 kcal mol^{-1} according to the Eyring equation). However, compared to results obtained by ab initio calculations, PM3 gives about 5−10 kcal mol^{-1} higher activation energies for proton transfer reactions with nitrogen-containing reactants.[72] In a study of the reaction mechanism of citrate synthase using calculations on a model system (5-methylimidazole and methylthioacetate representing histidine and the enolate of acetyl-CoA) at various ab initio levels and with semiempirical methods, Mulholland et al. found similar activation energy differences for the proton transfer reaction.[73] Thus, the absolute values of the PM3 energies obtained in this work should not be overstressed, but, nevertheless, they allow a clear choice between the two proposed reaction mechanisms.

Another aspect that should be taken into account is that a significant contribution of quantum-mechanical tunneling for hydrogen transfer reactions in proteins is expected.[74−76] In the case of liver alcohol dehydrogenase, it has been suggested that tunneling makes a contribution of 80% to the hydrogen transfer process.[76,77] Especially if the energies of the reactants and products are nearly equal and if the hydrogen atom has to pass a narrow and high barrier, tunneling gains importance compared to the classical, thermally activated mechanism.[74,76] Furthermore, it has been suggested that thermal fluctuations in the protein structure increase the tunneling probability by shortening the distance that the hydrogen atom has to move. These conditions can be found in the active site of PLA_2. The active site structure has proved to be very flexible, and, for the tetrahedral intermediate, the transition state of the decomposition step and the product structure more than one minimum geometry has been determined. Furthermore, the distance between Nδ1 of His48 and the ester oxygen of the substrate in the transition state structure is only 2.59 Å, because the imidazole ring of His48 and the substrate move toward each other. The distance through which the hydrogen atom has to pass is, therefore, only about 0.6 Å. This indicates strongly that hydrogen tunneling makes a significant contribution to the decomposition step of the hydrolysis. However, this aspect is the topic of further investigations.

Taking steric and long-range electrostatic interactions of the protein environment into account, the calculations clearly show that the environment has a large influence on the whole enzymatic reaction. The reaction pathways determined for the ester hydrolysis depend on the size of the model system. In the systems $\mathbf{4_8}-\mathbf{4_1}$ the decomposition step is rate-limiting, while the formation of the tetrahedral intermediate is the rate-limiting step in systems $\mathbf{1}-\mathbf{3}$, $\mathbf{4_0}$, and $\mathbf{4_{78}}$. The energy profiles obtained by calculations with different dielectric constants (Figure 12) show that the stabilization of the tetrahedral intermediate amounts to 8 kcal mol^{-1} for $\epsilon = 78$ (system $\mathbf{4_{78}}$), 11 kcal mol^{-1} for $\epsilon = 4$ (system $\mathbf{4_4}$), and to 21 kcal mol^{-1} for $\epsilon = 1$ (system $\mathbf{4_1}$). The relative energy of the tetrahedral intermediate in the minimal model (system **1**), which has no environment at all, is 40 kcal mol^{-1} higher than the relative energy of the corresponding geometry of system $\mathbf{4_4}$.

Acknowledgment. We thank the Deutsche Forschungsgemeinschaft for financial support. Special thanks go to Anselm Horn and Torsten Schindler for their generous VAMP support.

References and Notes

(1) Warshel, A.; Åqvist, J. *Annu. Rev. Biophys. Biophys. Chem.* **1991**, *20*, 267.
(2) Warshel, A.; Levitt, M. *J. Mol. Biol.* **1976**, *103*, 227.
(3) Singh, U. C.; Kollmann, P. A. *J. Comput. Chem.* **1986**, *7*, 718.
(4) Field, M. J.; Bash, P. A.; Karplus, M. *J. Comput. Chem.* **1990**, *11*, 700.
(5) Gao, J. Methods and applications of combined quantum mechanical and molecular mechanical potentials. In *Reviews of Computational Chemistry*; Lipkowitz, K. B., Boyd, D. B., Eds.; VCH Publishers: New York, 1996; Vol. 7, pp 119−185.
(6) Mordasini, T. Z.; Thiel, W. *Chimia* **1998**, *58*, 288.
(7) Hart, J. C.; Burton, N. A.; Hillier, I. H.; Harrison, M. J.; Jewsbury, P. *Chem. Commun.* **1997**, 1431.
(8) Kolmodin, K.; Åqvist, J. *Int. J. Quantum Chem.* **1999**, *73*, 147.
(9) Lyne, P. D.; Mulholland, A. J.; Richards, W. G. *J. Am. Chem. Soc.* **1995**, *117*, 11345.
(10) Moliner, V.; Andrés, J.; Oliva, M.; Safont, V. S., Tapia, O. *Theor. Chem. Acc.* **1999**, *101*, 228.
(11) Moliner, V.; Turner, A. J.; Williams, I. H. *Chem. Commun.* **1997**, 1271.
(12) Mulholland, A. J.; Richards, W. G. *Proteins* **1997**, *27*, 9.

(13) Ranganathan, S.; Gready, J. E. *J. Phys. Chem. B* **1997**, *101*, 5614.
(14) Ridder, L.; Mulholland, A. J.; Vervoort, J.; Rietjens, I. M. C. M. *J. Am. Chem. Soc.* **1998**, *120*, 7641.
(15) Ramos, M. J.; Melo, A.; Henriques, E. S.; Gomes, J. A. N. F.; Reuter, N.; Maigret, B.; Floriano, W. B.; Nascimento, M. A. C. *Int. J. Quantum Chem.* **1999**, *74*, 299.
(16) Toba, S.; Damodaran, K. V.; Merz, K. M., Jr. *J. Med. Chem.* **1999**, *42*, 1225.
(17) Åqvist, J.; Warshel, A. *Chem. Rev.* **1993**, *93*, 2523.
(18) Eurenius, K. P.; Chatfield, D. C.; Brooks, B. R.; Hodoscek, M. *Int. J. Quantum Chem.* **1996**, *60*, 1189.
(19) Monard, G.; Merz, K. M., Jr. *Acc. Chem. Res.* **1999**, *32*, 904.
(20) Waskowycz, B.; Hillier, I. H.; Gensmantel, N.; Payling, D. W. *J. Chem. Soc., Perkin Trans. 2* **1991**, 225.
(21) Heitler, W.; London, F. *Z. Physik* **1927**, *44*, 455.
(22) Grochowski, P.; Lesyng, B.; Bala, P.; McCammon, J. A. *Int. J. Quantum Chem.* **1996**, *60*, 1143.
(23) Bala, P.; Grochowski, P.; Lesyng, B.; McCammon, J. A. QCMD. Models and Applications. In *Quantum Mechanical Simulation Methods for Studying Biological Systems*; Bicout, D., Field, M., Eds.; Springer-Verlag: Berlin, Heidelberg, New York, 1996; 119−157.
(24) Warshel, A.; Weiss, R. M. *J. Am. Chem. Soc.* **1980**, *102*, 6218.
(25) Clark, T.; Gedeck, P.; Lanig, H.; Schürer, G. Semiempirical MO Calculations on Enzyme Reaction Mechanisms. In *Molecular Modeling and Dynamics of Bioinorganic Systems*; Banci, L., Comba, P., Eds.; Kluwer Academic Publishers: Dordrecht, 1997; pp 307−317.
(26) Clark, T.; Alex, A.; Beck, B.; Gedeck, P.; Lanig, H. *J. Mol. Model.* **1999**, *5*, 1.
(27) Tibes, U.; Friebe W.-G. *Exp. Opin. Invest. Drugs* **1997**, *6*, 279.
(28) Jain, M. K.; Gelb, M. H.; Rogers, J.; Berg, O. G. *Methods Enzymol.* **1995**, *249*, 567.
(29) Clausen-Schaumann, H.; Grandbois, M.; Gaub, H. E. *Adv. Mater.* **1998**, *10*, 949.
(30) Dijkstra, B. W.; Drenth, J.; Kalk, K. H.; Vandermaelen, P. J. *J. Mol. Biol.* **1978**, *124*, 53.
(31) The numbering of the residues is taken from the homology numbering based on bovine pancreas PLA2, as usually used in the literature, and not from the original PDB entry.
(32) Dijkstra, B. W.; Drenth, J.; Kalk, K. H. *Nature* **1981**, *289*, 604.
(33) Dijkstra, B. W.; Kalk, K. H.; Hol, W. G. J.; Drenth, J. *J. Mol. Biol.* **1981**, *147*, 97.
(34) Dijkstra, B. W.; Renetseder, R.; Kalk, K. H.; Hol, W. G. J.; Drenth, J. *J. Mol. Biol.* **1983**, *168*, 163.
(35) Dijkstra, B. W.; Drenth, J.; Kalk, K. H.; de Haas, G. H.; Egmond, M. R.; Slotboom, A. J. *Biochemistry* **1984**, *23*, 2759.
(36) Li, Y.; Tsai, M.-D. *J. Am. Chem. Soc.* **1993**, *115*, 8523.
(37) Liu, X.; Zhu, H.; Huang, B.; Rogers, J.; Yu, B.-Y.; Kumar, A.; Jain, M. K.; Sundraralingam, M.; Tsai, M.-D. *Biochemistry* **1995**, *34*, 7322.
(38) Verheij, H. M.; Volwerk, J. J.; Jansen, E. H. J. M.; Puyk, W. C.; Drenth, J.; de Haas, G. H. *Biochemistry* **1980**, *19*, 743.
(39) Chang L.-S.; Lin, S.-R.; Chang, C.-C. *J. Protein Chem.* **1996**, *15*, 701.
(40) Kuipers, O. P.; Dekker, N.; Verheij, H. M.; de Haas, G. H. *Biochemistry* **1990**, *29*, 6094.
(41) Jones, S. T.; Ahlström, P.; Berendsen, H. J. C.; Pickersgill, R. W. *Biochim. Biophys. Acta* **1993**, *1162*, 135.
(42) Seshadri, K.; Vishveshwara, S.; Jain, M. K. *Proc. Indian Acad. Sci.* **1994**, *106*, 1177.
(43) Einspahr, H.; Bugg, C. E. Crystal Structure Studies of Calcium Complexes and Implications for Biological Systems. In *Metal Ions in Biological Systems Vol 17; Calcium and its Role in Biology*; Sigel, H., Ed.; Marcel Dekker Inc.: New York, 1984; pp 51−97.
(44) Scott, D. L.; White, S. P.; Otwinowski, Z.; Yuan, W.; Gelb, M. H.; Sigler, P. B. *Science* **1990**, *250*, 1541.
(45) URL: http://www.rcsb.org/pdb. German mirror site: http://pdb.gmd.de.
(46) White, S. P.; Scott, D. L.; Otwinowski, Z.; Gelb, M. H.; Sigler, P. B. *Science* **1990**, *250*, 1560.
(47) Thunnissen M. G. M. M.; Ab, E.; Kalk, K. H.; Drenth, J.; Dijkstra, B. W.; Kuipers, O. P.; Dijkman, R.; de Haas, G. H.; Verheij, H. M. *Nature* **1990**, *347*, 689.
(48) Dennis, E. A. *Enzymes* **1983**, *16*, 307.
(49) Kumar, A.; Sekharudu, C.; Ramakrishnan, B.; Dupureur, C. M.; Zhu, H.; Tsai, M.-D.; Sundraralingam, M. *Protein Sci.* **1994**, *3*, 2082.
(50) Rogers, J.; Yu, B.-Z.; Serves, S. V.; Tsivgoulis, G. M.; Sotiropoulos, D. N.; Ioannou, P. V.; Jain, M. K. *Biochemistry* **1996**, *35*, 9375.
(51) Hart, H. *Organische Chemie: ein kurzes Lehrbuch*; VCH−Verlag: Weinheim, Basel, Cambridge, New York, 1989; p 267.
(52) Sekar, K.; Yu, B.-Z.; Rogers, J.; Lutton, J.; Liu, X.; Chem, X.; Tsai, M.-D.; Jain, M. K.; Sundaralingam, M. *Biochemistry* **1997**, *36*, 3104.
(53) Yu, B.-Z.; Rogers, J.; Nicol, G. R.; Theopold, K. H.; Seshadri, K.; Vishveshwara, S.; Jain, M. K. *Biochemistry* **1998**, *37*, 12576.
(54) Alex, A.; Clark, T. *J. Comput. Chem.* **1992**, *13*, 704.
(55) Fife, T. H.; Przystas, T. *J. Am. Chem. Soc.* **1986**, *108*, 4631.
(56) Hartmann, M.; Merz, K. M., Jr.; van Eldik, R.; Clark, T. *J. Mol. Model.* **1998**, *4*, 355.
(57) Onciul, A. von R.; Clark, T. *J. Comput. Chem.* **1993**, *14*, 392.
(58) Sloan, D. L.; Young, J. M.; Midvan, J. S. *Biochemistry* **1975**, *14*, 1998.
(59) Yu, B.-Z.; Berg, O. G.; Jain, M. K. *Biochemistry* **1993**, *32*, 6485.
(60) Schürer, G. Diploma Thesis, Universität Erlangen, 1997.
(61) Allinger, N. L. *J. Am. Chem. Soc* **1977**, *99*, 8127.
(62) Gasteiger, J.; Marsili, M. *Tetrahedron* **1980**, *36*, 3219.
(63) Cornell, W. D.; Cieplak, P.; Bayly, C. I.; Gould, I. R.; Merz, K. M., Jr.; Ferguson, D. M.; Spellmeyer, D. C.; Fox, T.; Caldwell, J. W.; Kollman, P. A. *J. Am. Chem. Soc.* **1995**, *117*, 5179.
(64) Clark, T.; Alex, A.; Beck, B.; Chandrasekar, J.; Gedeck, P.; Horn, A.; Hutter, M.; Martin, B.; Rauhut, G.; Sauer, W.; Schindler, T.; Steinke, T. *Program package VAMP 7.0*, Oxford Molecular Group Plc.: Oxford, 1998.
(65) Stewart, J. J. P. *J. Comput. Chem.* **1989**, *10*, 209.
(66) Wu, J.; Hehre, W. J. *J. Comput. Chem.*, to be submitted (implemented in SPARTAN from version 4.1 onward).
(67) Wery, J.-P.; Schevitz, R. W.; Clawson, D. K.; Bobbit, J. L.; Dow, E. R.; Gamboa, G.; Goodson, T., Jr.; Hermann, R. B.; Kramer, R. M.; McClure, D. B.; Mihelich, E. D.; Putnam, J. E.; Sharp, J. D.; Stark, D. H.; Teater, C.; Warrick, M. W.; Jones, N. D. *Nature* **1991**, *352*, 79.
(68) Warshel, A. *Computer Modeling of Chemical Reactions in Enzymes and in Solutions*; Wiley: New York, 1991.
(69) King, G.; Lee, F. S.; Warshel, A. *J. Chem. Phys.* **1991**, *95*, 4366.
(70) Beck, B.; Rauhut, G.; Clark, T. *J. Comput. Chem.* **1994**, *15*, 1064.
(71) Dupureur, C. M.; Deng, T.; Kwak, J.-G.; Noel, J. P.; Tsai, M.-D. *J. Am. Chem. Soc.* **1990**, *112*, 7074.
(72) Kallies, B.; Mitzner, R. *J. Mol. Model.* **1995**, *1*, 68.
(73) Mulholland, A. J.; Richards, W. G. *J. Phys. Chem. B* **1998**, *102*, 6635.
(74) Bruno, W. J.; Bialek, W. *Biophys. J.* **1992**, *63*, 689.
(75) Cha, Y.; Murray, C. J.; Klinman, J. P. *Science* **1989**, *243*, 1325.
(76) Klinman, J. P. *Trends Biochem. Sci.* **1989**, *9*, 368.
(77) Huskey, W. P.; Schowen, R. L. *J. Am. Chem. Soc.* **1983**, *105*, 5704.